

Master Degree in Computational and Applied Mathematics  
2024-2025

*Master Thesis*

# Leveraging Physics-Informed Neural Networks for Option Pricing Problems

---

Jose Pedro Melo Olivares

Madrid, 2025

## AVOID PLAGIARISM

The University uses the **Turnitin Feedback Studio** for the delivery of student work. This program compares the originality of the work delivered by each student with millions of electronic resources and detects those parts of the text that are copied and pasted. Plagiarizing in a TFM is considered a **Serious Misconduct**, and may result in permanent expulsion from the University.



This work is licensed under Creative Commons **Attribution - Non Commercial - Non Derivatives**



## SUMMARY

This thesis investigates the application of Physics-Informed Neural Networks (PINNs) to the pricing of financial derivatives governed by partial differential equations. Traditional numerical methods—such as finite-difference schemes and Monte Carlo simulations—face limitations when confronted with high-dimensional models, early-exercise features and complex market dynamics. PINNs offer a mesh-free alternative: by embedding the pricing partial differential equation (PDE) directly into the training loss of a neural network, they deliver efficient and flexible approximations.

We employ PINNs to price a range of derivatives—including European and American options, basket options and swaptions—under both the classical Black-Scholes assumptions and extensions with stochastic volatility and stochastic interest rates. Empirical results show that PINNs recover accurate pricing surfaces with low relative error, scale to higher dimensions, and provide significant speed-ups at inference time versus Monte Carlo methods. Training time and accuracy near payoff discontinuities remain challenges. Overall, this work highlights both the potential and the limits of PINNs in quantitative finance and outlines directions for future research on scalable, data-driven pricing methodologies.

**Keywords:** Physics-Informed Neural Networks, quantitative finance, option pricing, derivatives.



## CONTENTS

1. INTRODUCTION . . . . .	1
1.1. Motivation . . . . .	1
1.2. Objectives . . . . .	1
1.3. Thesis Structure . . . . .	2
2. THEORETICAL BACKGROUND . . . . .	3
2.1. Derivative Pricing Fundamentals . . . . .	3
2.2. Modelling Framework . . . . .	5
2.2.1. Feynman-Kac Representation . . . . .	5
2.2.2. The Black-Scholes Model . . . . .	6
2.2.3. Multi-Asset Extension of the Black–Scholes Model . . . . .	7
2.2.4. Stochastic Volatility Extension . . . . .	8
2.2.5. Stochastic Interest Rates Extension . . . . .	11
2.2.6. Joint Stochastic Volatility and Stochastic Rates . . . . .	12
2.3. Traditional Numerical Approaches . . . . .	12
3. PHYSICS-INFORMED MACHINE LEARNING . . . . .	15
3.1. Introduction to Physics-Informed Neural Networks (PINNs) . . . . .	15
3.2. Training PINNs . . . . .	15
4. IMPLEMENTATION AND RESULTS . . . . .	18
4.1. Implementation Details . . . . .	18
4.2. Call Option . . . . .	18
4.2.1. Multi-Asset Option . . . . .	22
4.2.2. Call Option with Stochastic Volatility and Interest Rates . . . . .	25
4.3. Put Option Pricing . . . . .	28
4.3.1. American Put Option Pricing . . . . .	30
4.4. Swaption Pricing . . . . .	31
5. DISCUSSION, LIMITATIONS, AND OUTLOOK . . . . .	34
5.1. Discussion of the Main Findings . . . . .	34
BIBLIOGRAPHY . . . . .	35



## LIST OF FIGURES

3.1	Collocation points for a put option. Points are sampled inside the domain $\Omega$ , on the boundary $\partial\Omega$ , and on the initial slice $\Omega_0$ . . . . .	16
3.2	Schematic of PINN training. (1) Collocation points are fed into the neural network. (2) Automatic differentiation yields spatial and temporal derivatives. (3) PDE residuals—and hence the loss terms—are evaluated at those points. (4) The resulting losses are combined to form $\mathcal{L}(\theta)$ ; its gradient drives an optimisation step on $\theta$ . The cycle repeats until convergence. . . . .	17
4.1	Call option price under the Black-Scholes PDE. The PINN solution closely matches the analytical benchmark. . . . .	19
4.2	Absolute error of the PINN solution. Errors peak close to maturity and the strike price. . . . .	20
4.3	Solution at expiry. The PINN solution closely matches the analytical benchmark, except around the strike price where the absolute error peaks. . . . .	21
4.4	Relative error of the PINN solution. The error is concentrated around the strike price and maturity. . . . .	21
4.5	Dimensionless multi-asset call option price (first two asset axes). . . . .	23
4.6	Multi-asset call option price in original coordinates (first two asset axes). . . . .	23
4.7	Seven-asset call option surfaces for two architectures. The network with 60 neurons per layer captures the solution more faithfully than the smaller 10-neuron model. . . . .	24
4.8	Training loss for multi-asset PINNs. Higher dimensions slow convergence and flatten the loss curve. The smaller network sometimes terminates early, yielding a shorter training time but a noticeably larger error. . . . .	24
4.9	CPU timing comparison between PINN inference and Monte Carlo simulation (50000 simulations). . . . .	25
4.10	Call option pricing surfaces using the Heston-Hull-White model for different volatility levels. . . . .	26
4.11	Price sensitivity to changes in volatility ( $v$ ). Higher values decrease curvature in the price surface. . . . .	27
4.12	Price sensitivity to short rates in the Heston-Hull-White model. Higher interest rates raise the option's hedging cost, increasing the option price. . . . .	27

4.13	Price surface at $t = 0$ for the stock and volatility dimension.	28
4.14	Price surface at $t = 0$ for the stock and volatility dimension.	28
4.15	European put option pricing: comparison between PINN (left) and analytical Black-Scholes solution (right).	29
4.16	Absolute error distribution for the European put option. Errors peak around maturity near the strike price.	29
4.17	American put option prices: PINN solution (left) compared to a numerical benchmark solution (right).	30
4.18	Absolute error for American put option pricing. Errors primarily arise around the dynamic early-exercise boundary.	31
4.19	European payer swaption pricing surface. Left: PINN solution. Right: reference solution computed with an analytic approximation or semi-analytical method.	32
4.20	Absolute error in pricing the European payer swaption. The error is primarily concentrated near expiry and around the strike.	33



## **LIST OF TABLES**

4.1	Call Option Parameters . . . . .	19
4.2	Multi-Asset Call Option Parameters . . . . .	22
4.3	Parameters for the Call Option under the Heston-Hull-White Model . . .	26



# 1. INTRODUCTION

## 1.1. Motivation

The rapid progress in machine learning over the past decade has transformed fields such as speech recognition, image recognition and object detection [1]. The financial industry likewise seeks innovative, accurate computational methods to price complex products. Derivatives—whose value depends on underlying assets [2]—are central to risk management, speculative trading and hedging.

Derivatives reference a wide range of assets, including equities, bonds, commodities and indices [3]. Accurate pricing informs both investment decisions and risk control. Historically, practitioners relied on Monte Carlo (MC) simulation [4] or on partial differential equations (PDEs) such as Black-Scholes [5]. While PDE-based methods yield theoretical insight, their application is curtailed by the curse of dimensionality [6].

The emergence of Physics-Informed Neural Networks (PINNs) [7] offers a novel approach. Exploiting the universal-approximation capability of neural networks, PINNs embed the governing PDE directly into the learning objective. This allows the network to learn from the mathematical structure of the problem, ensuring consistency with financial theory while reducing training time. The approach is particularly attractive to institutions that require real-time pricing for complex derivatives.

PINNs can also generate complete price surfaces instantaneously, enabling immediate sensitivity analysis and risk assessment across broad market scenarios—e.g. valuation adjustments (XVA) or internal-model frameworks.

This master’s thesis explores and validates the use of PINNs in derivative pricing. Guided by professionals at BBVA, the research assesses whether PINNs can efficiently and accurately price complex derivatives through PDEs and thus be adopted in practice.

## 1.2. Objectives

The overarching aim of this thesis is two-fold. First, we investigate the suitability of Physics-Informed Neural Networks (PINNs) for pricing financial derivatives with a variety of underlying dynamics and pay-off structures. Second, we evaluate whether PINNs can serve as a competitive alternative to traditional numerical procedures—most notably Monte-Carlo simulation and finite-difference schemes.

More concretely, the work pursues three specific objectives:

- **Theoretical review:** present the foundations of derivative pricing and derive the associated partial-differential equations (PDEs) for a representative set of products.

- **Classical benchmarks:** summarise the main numerical techniques used to solve these PDEs—finite differences and Monte-Carlo—and highlight their practical limitations.
- **PINN assessment:** measure the accuracy, computational efficiency and scalability of PINNs when pricing both single-asset and multi-asset derivatives.

Beyond these technical goals, the thesis seeks to provide insights of direct relevance to the financial industry—drawing on guidance from professionals at BBVA—and to contribute to the growing body of research that bridges deep learning and quantitative finance.

### 1.3. Thesis Structure

The manuscript is organised into six chapters, each addressing a distinct aspect of the study:

- **Chapter 1: Introduction**  
Sets out the motivation, states the objectives, and outlines the thesis structure.
- **Chapter 2: Theoretical Background**  
Reviews the fundamentals of derivative pricing, from the Black-Scholes model to common extensions, and surveys classical numerical methods together with their shortcomings.
- **Chapter 3: Physics-Informed Neural Networks**  
Introduces the neural-network concepts underpinning PINNs, details their architecture, and explains the training procedure used to enforce the governing PDEs and constraints.
- **Chapter 4: Implementation and Results**  
Describes the computational set-up and reports empirical results for the different PDEs and instruments considered, analysing the performance of PINNs in terms of accuracy and speed.
- **Chapter 5: Conclusions and Future Work**  
Summarises the key findings, discusses limitations, and proposes directions for future research on PINN-based pricing.

## 2. THEORETICAL BACKGROUND

This chapter provides the foundational concepts necessary for understanding how financial products are priced, as well as the mathematical tools traditionally used for their valuation. It begins by introducing derivatives and the types most commonly traded in financial markets, then discusses the theoretical models used to price them and the limitations of classical numerical methods.

### 2.1. Derivative Pricing Fundamentals

Financial derivatives are contracts whose cash flows, or payments, are linked to the value of one or several *underlyings*—such as shares, commodities, foreign exchange rates, or interest rates [2], [3]. These instruments enable market participants to insure portfolios, manage exposure to financial risks, or express directional views.

The starting point for almost every derivatives textbook is the European call or put option. A European call option gives, at a fixed future date  $T$ , the right to buy the underlying at the pre-agreed strike price  $K$ ; a European put option grants the right to sell the underlying asset at the same strike. The payoff functions

$$\max(S_T - K, 0), \quad \max(K - S_T, 0)$$

characterise this optionality and depend only on the future spot price  $S_T$ . Valuing the contract amounts to forecasting the *distribution* of  $S_T$  under a special probability measure that allows the counterparties to eliminate, or *hedge*, the risks associated with movements in the underlying asset. The Black–Scholes formula achieves this under a set of assumptions, for example that the underlying follows a geometric Brownian motion with constant drift and volatility. Under these assumptions, the call price is given by the closed-form expression

$$C(S_t, K, T) = S_t N(d_1) - K e^{-r(T-t)} N(d_2),$$

where  $N$  is the cumulative distribution function of the standard normal distribution,  $r$  is the risk-free interest rate, and

$$d_1 = \frac{\ln(S_t/K) + (r + \sigma^2/2)(T - t)}{\sigma \sqrt{T - t}}, \quad d_2 = d_1 - \sigma \sqrt{T - t}.$$

The Black–Scholes model is a cornerstone of modern finance, but its assumption of constant volatility is often too simplistic for real-world markets. Empirical evidence shows that volatility frequently varies over time, prompting practitioners to enhance the basic model by treating volatility itself as random or dynamic [8]. Although these modifications make the pricing equations more realistic, they no longer yield simple closed-form

solutions, thus requiring numerical methods—such as finite differences, Monte Carlo simulations, Fourier integrals, or, as this thesis investigates, Physics-Informed Neural Networks (PINNs).

However, not all financial derivatives fit neatly into this framework. For instance, American options differ from European ones by allowing the holder to exercise at any time up to expiry, adding complexity because the optimal exercise time becomes part of the pricing problem. Technically, valuation transforms into a free-boundary problem in which one must determine both the option price and the moving boundary that separates the hold and exercise regions. Traditional numerical approaches—tree methods, finite-difference schemes, or regression-based Monte Carlo—tend to suffer from slow convergence or high variance.

Similarly, basket options—which derive value from multiple underlying assets—introduce another layer of complexity. Such contracts, commonly found in structured products, depend heavily on the joint behaviour of the underlyings. The payoff may, for example, depend only on the best-performing asset in a basket, making valuation challenging because complexity grows exponentially as additional assets are included. This "curse of dimensionality" makes traditional finite-difference methods impractical and Monte Carlo simulations noisy, further motivating advanced techniques such as high-dimensional PINNs.

Complexity continues to rise with *long-dated equity or FX options*, which are sensitive not only to the underlying asset price but also to volatility dynamics and varying interest rates. One way to address this is to combine stochastic-volatility models, which capture realistic volatility dynamics, with interest-rate models that discount future cash flows accurately. Individually manageable, these factors together create intricate, multi-dimensional valuation problems without straightforward analytic solutions.

Moreover, unlike equity or FX derivatives tied to a single traded asset, *interest-rate derivatives* such as *payer swaptions* depend on the evolution of an entire yield curve. A payer swaption grants its holder the right, at a future date  $T$ , to lock in a fixed rate  $K$  on an interest-rate swap spanning from  $T$  to a final maturity  $T_n$ . At expiry, if the prevailing market swap rate  $L(T)$  exceeds  $K$ , the option is exercised; otherwise, it expires worthless. The payoff therefore equals the present value of future fixed-versus-floating payments, scaled by  $\max(L(T) - K, 0)$ . Pricing thus requires a model that simultaneously fits current discount curves and realistically forecasts their evolution.

Simplified models such as the one-factor Hull–White approach partially achieve this balance, yet closed-form solutions disappear once real-world constraints (e.g., callability or collateral requirements) are introduced, forcing practitioners to rely on numerical integration or other flexible numerical methods. PINNs emerge as an attractive alternative, seamlessly integrating curve fitting and pricing within a single computational framework.

From the plain European call to complex structures such as American options, basket contracts, and swaptions, each derivative type adds incremental complexity: multiple underlyings, additional risk factors, early-exercise features, yield-curve dependencies, and

more. Collectively, these complications erode the neat closed-form solutions of classical theory and push traditional numerical methods beyond practicality.

By contrast, PINNs offer a mesh-free, dimension-agnostic alternative that naturally incorporates boundary or inequality constraints through their loss functions. The remainder of this thesis systematically quantifies how these desirable properties translate into gains in computational speed, flexibility, and accuracy across five representative derivative contracts [9], [10].

## 2.2. Modelling Framework

Financial derivatives can be valued in two complementary ways. On the one hand, the price equals the discounted expectation of the payoff under a risk-neutral probability measure  $\mathbb{Q}$ ; on the other, it is the unique solution of a specific partial differential equation (PDE). The Feynman–Kac theorem builds a bridge between these stochastic and analytic representations: once the appropriate state vector has been specified, it turns a conditional expectation into a PDE, and vice versa.

This equivalence is the backbone of the chapter. We first state the general Feynman–Kac theorem and then use it as a template to derive the PDEs associated with increasingly rich models: the Black–Scholes geometric Brownian motion, its correlated multi-asset extension, and further variants that incorporate stochastic volatility and stochastic interest rates.

### 2.2.1. Feynman–Kac Representation

The multidimensional Feynman–Kac theorem, a fundamental result linking PDEs to stochastic processes, is presented here in a financial context. Under standard regularity assumptions, the value function  $u : [0, T] \times \mathbb{R}^d \rightarrow \mathbb{R}$  that solves

$$\frac{\partial u}{\partial t} + \frac{1}{2} \sum_{i=1}^d \sum_{j=1}^d \rho_{ij} \sigma_i(t, \mathbf{x}) \sigma_j(t, \mathbf{x}) x_i x_j \frac{\partial^2 u}{\partial x_i \partial x_j} + \sum_{i=1}^d \mu_i(t, \mathbf{x}) x_i \frac{\partial u}{\partial x_i} - r_t u = 0, \quad (2.1)$$

$$u(T, \mathbf{x}) = \Phi(\mathbf{x}),$$

admits the probabilistic representation

$$u(t, \mathbf{x}) = \mathbb{E}^{\mathbb{Q}} \left[ e^{- \int_t^T r_s ds} \Phi(\mathbf{X}_T) \mid \mathbf{X}_t = \mathbf{x} \right], \quad (2.2)$$

where the state process  $\mathbf{X}_t = (X_t^{(1)}, \dots, X_t^{(d)})$  follows the correlated geometric Itô diffusion

$$dX_t^{(i)} = \mu_i(t, \mathbf{X}_t) X_t^{(i)} dt + \sigma_i(t, \mathbf{X}_t) X_t^{(i)} dW_t^{(i)}, \quad i = 1, \dots, d, \quad (2.3)$$

with quadratic covariations  $dW_t^{(i)} dW_t^{(j)} = \rho_{ij} dt$ . Here  $\mu_i$  and  $\sigma_i$  are (possibly state- and time-dependent) drift and volatility functions,  $r_t$  is the short-rate process,  $\rho$  is the constant correlation matrix, and  $\Phi$  specifies the terminal payoff at maturity  $T$ .

## 2.2.2. The Black-Scholes Model

We begin by briefly reviewing the framework proposed by Black and Scholes [11]. They assumed that the underlying asset price  $(S_t)_{t \geq 0}$  evolves according to a geometric Brownian motion described by the stochastic differential equation (SDE):

$$dS_t = \mu S_t dt + \sigma S_t dW_t^{\mathbb{P}}, \quad S_0 > 0, \quad (2.4)$$

where  $\mu$  denotes the expected return under the real-world measure  $\mathbb{P}$  and  $\sigma$  is the asset volatility.

The key insight behind derivative pricing is the construction of a hedged portfolio:

$$\Pi_t = V(t, S_t) - \Delta_t S_t,$$

where  $V(t, S_t)$  is the derivative price and  $\Delta_t$  denotes the quantity of the underlying asset held. By applying Ito's lemma, it can be shown that choosing

$$\Delta_t = \frac{\partial V}{\partial S}$$

makes the portfolio instantaneously risk-free. Consequently, it must earn the risk-free rate  $r$ , leading to the well-known *Black–Scholes PDE*:

$$\frac{\partial V}{\partial t} + \frac{1}{2} \sigma^2 S^2 \frac{\partial^2 V}{\partial S^2} + rS \frac{\partial V}{\partial S} - rV = 0, \quad (2.5)$$

with terminal condition  $V(T, S) = \Phi(S)$ , where all partial derivatives are evaluated at  $(t, S_t)$ . The Feynman–Kac theorem in the Black–Scholes setting reduces to

$$V(t, S) = e^{-r(T-t)} \mathbb{E}^{\mathbb{Q}}[\Phi(S_T) | S_t = S],$$

where the risk-neutral dynamics simplify to

$$dS_t = rS_t dt + \sigma S_t dW_t^{\mathbb{Q}}. \quad (2.6)$$

An important observation in (2.6) is that the drift term—in the risk-neutral measure  $\mathbb{Q}$ —equals the risk-free rate  $r$ . This result applies to any derivative we consider in this thesis, as it is a consequence of the *no-arbitrage principle*.

### Boundary Conditions

To solve the PDE for specific derivatives, appropriate boundary conditions must be defined. Practitioners define some as follows:

- **Terminal condition:** At maturity  $T$ ,

$$V(T, S) = \Phi(S).$$

For example, a European call option would have  $\Phi(S) = \max(S - K, 0)$ .

- **Lower boundary** ( $S \rightarrow 0$ ): As the asset price approaches zero, it is safe to assume that for a call option

$$V(t, 0) = 0,$$

but a more general approach is to set the option value independent of the underlying, resulting in

$$\frac{\partial V}{\partial t} - rV = 0.$$

- **Upper boundary** ( $S \rightarrow \infty$ ): For large underlying asset prices, the option price grows approximately linearly with the asset price, leading to

$$\frac{\partial^2 V}{\partial S^2} \rightarrow 0, \quad S \rightarrow \infty.$$

Boundary conditions for other derivatives can be found in standard references such as [3].

### 2.2.3. Multi-Asset Extension of the Black–Scholes Model

We now extend the Black–Scholes framework to the case of  $d \geq 2$  underlying assets. Setting the appropriate hedging weights  $\Delta_t = (\Delta_t^1, \dots, \Delta_t^d)^\top$  and repeating the replication argument from the single-asset case, one finds that, under the risk-neutral measure  $\mathbb{Q}$ , each asset earns the risk-free rate  $r$ . Hence the price vector  $\mathbf{S}_t = (S_t^1, \dots, S_t^d)^\top$  satisfies

$$dS_t^i = rS_t^i dt + \sigma_i S_t^i dW_t^{\mathbb{Q},i}, \quad dW_t^{\mathbb{Q},i} dW_t^{\mathbb{Q},j} = \rho_{ij} dt, \quad 1 \leq i, j \leq d. \quad (2.7)$$

Let  $V(t, \mathbf{S})$  denote the option value. The same hedging argument gives the PDE

$$\frac{\partial V}{\partial t} + \frac{1}{2} \sum_{i=1}^d \sum_{j=1}^d \sigma_i \sigma_j \rho_{ij} S_i S_j \frac{\partial}{\partial S_i S_j} + r \sum_{i=1}^d S_i \partial_{S_i} - rV = 0. \quad (2.8)$$

### Dimensionless Backward Equation

Training PINNs require appropriate input scaling and loss transformation in order to avoid numerical stability issues. A wise choice is to transform the PDE (2.8) into a dimensionless form. Formally, for maturity  $T$  define

$$x_k = \ln \frac{S_k}{K}, \quad \tau = T - t, \quad u(\tau, \mathbf{x}) = \frac{V(t, \mathbf{S})}{K},$$

where  $\mathbf{S} = (S_1, \dots, S_d)^\top$  and  $K$  is the strike. Starting from the multi-asset Black–Scholes PDE and applying the above change of variables, the chain rule yields the *dimensionless backward equation*

$$\frac{\partial u}{\partial \tau} = \frac{1}{2} \sum_{i=1}^d \sigma_i^2 \left( \frac{\partial^2 u}{\partial x_i^2} - \frac{\partial u}{\partial x_i} \right) + \frac{1}{2} \sum_{i=1}^d \sum_{j=1}^d \sigma_i \sigma_j \rho_{ij} \frac{\partial^2 u}{\partial x_i \partial x_j} + r \sum_{i=1}^d \frac{\partial u}{\partial x_i} - ru. \quad (2.9)$$

to be solved for  $\tau \in (0, T]$  and  $\mathbf{x} \in \mathbb{R}^d$  with terminal condition  $u(0, \mathbf{x}) = \Phi(\mathbf{x})/K$ . Equation (2.9) will serve as the reference problem for PINN solver in Section 2.2.3.

## Boundary Conditions

To solve the multi-asset case described above via the PDE (2.9) is a significant challenge due to the complexity of the boundary conditions. These conditions appear as an extension of the single-asset case and are explained below.

- **Terminal condition:** At maturity  $T$ , the option value is given by the payoff function of the dimensionless problem:

$$u(0, \mathbf{x}) = \Phi(\mathbf{x})/K,$$

where  $\Phi$  is the payoff function of the option in dimensionless form. In this thesis we will focus on the case of the best-of-basket option, which has the dimensionless payoff

$$\Phi(\mathbf{x}) = \max\left(\max_{1 \leq k \leq d} e^{x_k} - 1, 0\right).$$

- **Lower boundaries ( $S_k \rightarrow 0$ ):** As the underlying asset price  $S_k$  approaches zero, the option behaves as the  $d - 1$ -asset case. This is equivalent to solving (2.9) but removing the asset  $S_k$  from the problem. Mathematically, the boundary condition is given by:

$$\frac{\partial u}{\partial \tau} = \frac{1}{2} \sum_{\substack{i=1 \\ i \neq k}}^d \sigma_i^2 \left( \frac{\partial^2 u}{\partial x_i^2} - \frac{\partial u}{\partial x_i} \right) + \frac{1}{2} \sum_{\substack{i=1 \\ i \neq k}}^d \sum_{\substack{j=1 \\ j \neq k}}^d \sigma_i \sigma_j \rho_{ij} \frac{\partial^2 u}{\partial x_i \partial x_j} + r \sum_{\substack{i=1 \\ i \neq k}}^d \frac{\partial u}{\partial x_i} - ru.$$

- **Upper boundaries ( $S_k \rightarrow \infty$ ):** In the limit where the underlying asset price  $S_k$  becomes very large, we also want the option to behave linearly with respect to the underlying asset price  $S_k$ . As now we are working with dimensionless variables, we need to ensure that  $\frac{\partial^2 V}{\partial S_k^2} = 0$  is appropriately scaled. The resulting condition is

$$\frac{\partial u}{\partial \tau} = \frac{1}{2} \sum_{\substack{i=1 \\ i \neq k}}^d \sigma_i^2 \left( \frac{\partial^2 u}{\partial x_i^2} - \frac{\partial u}{\partial x_i} \right) + \frac{1}{2} \sum_{\substack{i=1 \\ i \neq k}}^d \sum_{\substack{j=1 \\ j \neq k}}^d \sigma_i \sigma_j \rho_{ij} \frac{\partial^2 u}{\partial x_i \partial x_j} + r \sum_{i=1}^d \frac{\partial u}{\partial x_i} - ru.$$

### 2.2.4. Stochastic Volatility Extension

As noted earlier, the Black–Scholes assumption of constant volatility and deterministic interest rates is often inadequate, especially for longer-dated equity and foreign-exchange options. Market-implied volatilities vary by strike and maturity, while the yield curve itself fluctuates with economic conditions and monetary policy. To reflect these dynamics, practitioners introduce *stochastic volatility* and *stochastic interest rates*, allowing models to match observed prices and to capture the joint sensitivity of derivatives to the underlying level, volatility changes, and rate movements.

Several routes lead to the desired pricing PDE; here we follow the hedging argument, so that later sections can invoke the Feynman-Kac theorem to obtain the corresponding probabilistic representation.

Working under the physical measure  $\mathbb{P}$ , assume

$$\begin{aligned} dS_t &= \mu S_t dt + \sqrt{v_t} S_t dW_t^{\mathbb{P},S}, \\ dv_t &= \kappa(\theta - v_t) dt + \sigma_v \sqrt{v_t} dW_t^{\mathbb{P},v}, \\ dW_t^{\mathbb{P},S} dW_t^{\mathbb{P},v} &= \rho dt, \end{aligned} \quad (2.10)$$

where  $\mu$  is the physical drift of the stock,  $\kappa$  the mean-reversion speed of the variance, and  $\theta$  its long-run level. Let  $V(t, S, v)$  be the value of the contract to price, and let  $\widehat{V}(t, S, v)$  be a second, traded option chosen for its sensitivity to  $v$ . Construct the self-financing portfolio

$$\Pi_t = V_t - \Delta_t S_t - \Phi_t \widehat{V}_t, \quad (2.11)$$

where  $\Delta_t$  and  $\Phi_t$  denote (short) positions in the underlying and in the auxiliary option, respectively. The diffusion of the portfolio is

$$d\Pi_t = dV_t - \Delta_t dS_t - \Phi_t d\widehat{V}_t, \quad (2.12)$$

and we analyse each component. Applying Ito's lemma to  $V$  and  $\widehat{V}$  and substituting

$$\begin{aligned} dV &= \left( \frac{\partial V}{\partial t} + \mathcal{L}^{\mathbb{P}} V \right) dt + \frac{\partial V}{\partial S} \sqrt{v} S dW_t^{\mathbb{P},S} + \frac{\partial V}{\partial v} \sigma_v \sqrt{v} dW_t^{\mathbb{P},v}, \\ d\widehat{V} &= \left( \frac{\partial \widehat{V}}{\partial t} + \mathcal{L}^{\mathbb{P}} \widehat{V} \right) dt + \frac{\partial \widehat{V}}{\partial S} \sqrt{v} S dW_t^{\mathbb{P},S} + \frac{\partial \widehat{V}}{\partial v} \sigma_v \sqrt{v} dW_t^{\mathbb{P},v}, \end{aligned} \quad (2.13)$$

where

$$\mathcal{L}^{\mathbb{P}} = \mu S \frac{\partial}{\partial S} + \kappa(\theta - v) \frac{\partial}{\partial v} + \frac{1}{2} v S^2 \frac{\partial^2}{\partial S^2} + \rho \sigma_v v S \frac{\partial^2}{\partial S \partial v} + \frac{1}{2} \sigma_v^2 v \frac{\partial^2}{\partial v^2}.$$

Substituting (2.13) into (2.12) and rearranging, the stochastic part of  $d\Pi_t$  becomes

$$\left[ \frac{\partial V}{\partial S} - \Delta_t - \Phi_t \frac{\partial \widehat{V}}{\partial S} \right] \sqrt{v} S dW_t^{\mathbb{P},S} + \left[ \frac{\partial V}{\partial v} - \Phi_t \frac{\partial \widehat{V}}{\partial v} \right] \sigma_v \sqrt{v} dW_t^{\mathbb{P},v}.$$

Setting each bracket to zero eliminates both Brownian terms. From the  $dW_t^{\mathbb{P},v}$  term we obtain

$$\Phi_t = \frac{\partial V / \partial v}{\partial \widehat{V} / \partial v}, \quad (2.14)$$

and from the  $dW_t^{\mathbb{P},S}$  term

$$\Delta_t = \frac{\partial V}{\partial S} - \Phi_t \frac{\partial \widehat{V}}{\partial S}. \quad (2.15)$$

With (2.14)–(2.15) the diffusion in  $\Pi_t$  is zero, so the drift of  $d\Pi_t$  must equal the risk-free rate:

$$d\Pi_t = r(V_t - \Delta_t S_t - \Phi_t \widehat{V}_t) dt. \quad (2.16)$$

Substituting (2.14), (2.15), and (2.13) into (2.12), and after some algebra, we obtain

$$\frac{\frac{\partial V}{\partial t} + \tilde{\mathcal{L}}V - rV}{\frac{\partial V}{\partial v}} = \frac{\frac{\partial \widehat{V}}{\partial t} + \tilde{\mathcal{L}}\widehat{V} - r\widehat{V}}{\frac{\partial \widehat{V}}{\partial v}}, \quad (2.17)$$

where

$$\tilde{\mathcal{L}} = rS \frac{\partial}{\partial S} + \kappa(\theta - v) \frac{\partial}{\partial v} + \frac{1}{2}vS^2 \frac{\partial^2}{\partial S^2} + \rho\sigma_v vS \frac{\partial^2}{\partial S \partial v} + \frac{1}{2}\sigma_v^2 v \frac{\partial^2}{\partial v^2}.$$

The only difference between  $\mathcal{L}^{\mathbb{P}}$  and  $\tilde{\mathcal{L}}$  is that the drift  $\mu$  has been replaced by the risk-free rate  $r$ .

Relation (2.17) must hold for *every* sufficiently smooth pair of payoffs  $(V, \widehat{V})$ , so the common value of the two quotients can depend *only* on the state variables  $(t, S, v)$ . We therefore introduce the *instantaneous market price of volatility risk*

$$\lambda(t, S, v) := \frac{\frac{\partial \widehat{V}}{\partial t} + \tilde{\mathcal{L}}\widehat{V} - r\widehat{V}}{\frac{\partial \widehat{V}}{\partial v}}$$

Substituting this definition into the numerator of (2.17) yields

$$\frac{\partial V}{\partial t} + \tilde{\mathcal{L}}V - rV = \lambda(t, S, v) \frac{\partial V}{\partial v}.$$

Collecting terms, we obtain the *risk-neutral* generator

$$\mathcal{L}^{\mathbb{Q}} = rS \frac{\partial}{\partial S} + [\kappa(\theta - v) - \lambda(t, S, v)] \frac{\partial}{\partial v} + \frac{1}{2}vS^2 \frac{\partial^2}{\partial S^2} + \rho\sigma_v vS \frac{\partial^2}{\partial S \partial v} + \frac{1}{2}\sigma_v^2 v \frac{\partial^2}{\partial v^2}.$$

Hence every European-style payoff  $V(t, S, v)$  satisfies

$$\frac{\partial V}{\partial t} + \mathcal{L}^{\mathbb{Q}}V - rV = 0, \quad V(T, S, v) = \Phi(S). \quad (2.18)$$

It is customary to assume that investors are *not* compensated for volatility risk, that is,  $\lambda(t, S, v) \equiv 0$ . The risk-neutral PDE then becomes

$$\frac{\partial V}{\partial t} + rS \frac{\partial V}{\partial S} + \kappa(\theta - v) \frac{\partial V}{\partial v} + \frac{1}{2}vS^2 \frac{\partial^2 V}{\partial S^2} + \rho\sigma_v vS \frac{\partial^2 V}{\partial S \partial v} + \frac{1}{2}\sigma_v^2 v \frac{\partial^2 V}{\partial v^2} - rV = 0. \quad (2.19)$$

By the Feynman-Kac theorem, the unique solution is

$$V(t, S, v) = e^{-r(T-t)} \mathbb{E}^{\mathbb{Q}} \left[ \Phi(S_T) \mid S_t = S, v_t = v \right], \quad (2.20)$$

where  $(S_t, v_t)_{t \in [0, T]}$  evolves according to

$$\begin{aligned} dS_t &= rS_t dt + \sqrt{v_t} S_t dW_t^{\mathbb{Q}, S}, \\ dv_t &= \kappa(\theta - v_t) dt + \sigma_v \sqrt{v_t} dW_t^{\mathbb{Q}, v}, \\ dW_t^{\mathbb{Q}, S} dW_t^{\mathbb{Q}, v} &= \rho dt, \end{aligned} \quad (2.21)$$

with parameters as defined above.

Because  $(S_t, v_t)$  is a two-dimensional Ito diffusion under  $\mathbb{Q}$ , the Feynman-Kac representation (2.20) holds without further hypotheses. In other words, once the risk-neutral SDEs (2.21) are fixed, the PDE follows automatically—a shortcut that will be invaluable for the extensions introduced later.

## Boundary Conditions

With stochastic volatility one must specify boundary conditions for extreme values of  $v$  [12]:

- **Lower boundary**  $v \rightarrow 0$ : As the volatility  $v$  approaches zero, there is no uncertainty in the underlying, therefore, we can set

$$V(t, S, 0) = e^{-(T-t)r} \Phi(S_T), \quad S_T = S_t e^{(T-t)r}.$$

- **Upper boundary**  $v \rightarrow \infty$ : As the volatility  $v$  becomes very large, the option price can move at most proportional to the underlying asset price  $S$ . This translates into the condition

$$\frac{\partial V}{\partial v} = S, \quad v \rightarrow \infty.$$

### 2.2.5. Stochastic Interest Rates Extension

For maturities beyond a few months, or for products whose underlying is an interest rate, treating the short rate as a constant is inadequate [13]. A more realistic approach lets the short rate  $r_t$  evolve stochastically, reflecting macroeconomic factors, monetary policy, and other market forces. Two widely used models are the *Vasicek* [14] and *Hull–White* [15] specifications. Both assume an Ornstein-Uhlenbeck, mean-reverting process, but the Hull-White model allows a time-dependent mean level, giving additional flexibility to fit the current yield curve.

Under the risk-neutral measure  $\mathbb{Q}$  both models can be written as

$$dr_t = \kappa(\theta(t) - r_t) dt + \sigma_r dW_t^{\mathbb{Q},r}, \quad (2.22)$$

where  $\kappa$  is the mean-reversion speed,  $\theta(t)$  the long-run level (constant for Vasicek, deterministic in  $t$  for Hull-White), and  $\sigma_r$  the volatility. For a derivative whose price is  $V(t, r)$ , the corresponding PDE is

$$\frac{\partial V}{\partial t} + \kappa(\theta(t) - r) \frac{\partial V}{\partial r} + \frac{1}{2} \sigma_r^2 \frac{\partial^2 V}{\partial r^2} - rV = 0. \quad (2.23)$$

A distinguishing feature of these short-rate models is their *affine* structure in the state variable  $r_t$ . In an affine model, key quantities such as bond prices can be expressed as exponentials of linear functions of the state, leading to closed-form solutions for zero-coupon bonds and related derivatives; see [13] for details.

## Boundary Conditions

Following [12], the boundary conditions in the  $r$ -dimension are

- $r \rightarrow \pm\infty$ : For very high or very low short rates the option price becomes insensitive to further changes in  $r$ , so

$$\frac{\partial V}{\partial r} = 0, \quad r \rightarrow \pm\infty.$$

### 2.2.6. Joint Stochastic Volatility and Stochastic Rates

Finally, we drop both the assumption of constant volatility and the assumption of constant interest rates, and consider a model that combines both factors as source of randomness. In this case, the joint dynamics of the state vector  $(S_t, v_t, r_t)$  under the risk-neutral measure  $\mathbb{Q}$  are given by the SDEs

$$\begin{aligned} dS_t &= r_t S_t dt + \sqrt{v_t} S_t dW_t^{\mathbb{Q},S}, \\ dv_t &= \kappa_v(\theta_v - v_t) dt + \sigma_v \sqrt{v_t} dW_t^{\mathbb{Q},v}, \\ dr_t &= \kappa_r(\theta_r(t) - r_t) dt + \sigma_r dW_t^{\mathbb{Q},r}, \\ dW_t^{\mathbb{Q},S} dW_t^{\mathbb{Q},v} &= \rho_{SV} dt, \\ dW_t^{\mathbb{Q},S} dW_t^{\mathbb{Q},r} &= \rho_{SR} dt, \\ dW_t^{\mathbb{Q},v} dW_t^{\mathbb{Q},r} &= \rho_{VR} dt, \end{aligned} \tag{2.24}$$

where  $\rho_{SV}, \rho_{SR}, \rho_{VR} \in [-1, 1]$  are the instantaneous correlations between the Brownian motions driving the dynamics of the underlying asset, the volatility, and the short rate, respectively. The corresponding pricing PDE for a derivative whose value depends on the state vector  $(S_t, v_t, r_t)$  is

$$\begin{aligned} \frac{\partial V}{\partial t} + \kappa_r(\theta_r(t) - r) \frac{\partial V}{\partial r} + \kappa_v(\theta_v - v) \frac{\partial V}{\partial v} + rS \frac{\partial V}{\partial S} - rV \\ + \rho_{SV}\sigma_v v S \frac{\partial^2 V}{\partial S \partial v} + \rho_{SR}\sigma_r S \sqrt{v} \frac{\partial^2 V}{\partial S \partial r} + \rho_{VR}\sigma_v \sigma_r \sqrt{v} \frac{\partial^2 V}{\partial v \partial r} \\ + \frac{1}{2}\sigma_r^2 \frac{\partial^2 V}{\partial r^2} + \frac{1}{2}vS^2 \frac{\partial^2 V}{\partial S^2} + \frac{1}{2}\sigma_v^2 v \frac{\partial^2 V}{\partial v^2} = 0. \end{aligned} \tag{2.25}$$

As no new dimensions are added compared to the previous sections, the boundary conditions are the same as in Section 2.2.4 and 2.2.5.

## 2.3. Traditional Numerical Approaches

### Overview of Finite Difference Methods

As noted earlier, Finite Difference Methods (FDM) are among the most widely used techniques for numerically solving partial differential equations such as (2.5) and their multi-dimensional counterpart (2.8). The idea is to discretise the time and asset-price domains into a structured grid and replace the continuous derivatives in the PDE with finite-difference approximations.

For instance, in the single-asset case the time derivative can be approximated with a backward difference:

$$\frac{\partial V}{\partial t} \approx \frac{V^n - V^{n-1}}{\Delta t},$$

while the first- and second-order spatial derivatives are obtained with central differences:

$$\frac{\partial V}{\partial S} \approx \frac{V_{i+1}^n - V_{i-1}^n}{2\Delta S}, \quad \frac{\partial^2 V}{\partial S^2} \approx \frac{V_{i+1}^n - 2V_i^n + V_{i-1}^n}{\Delta S^2}.$$

These substitutions turn the PDE into a system of algebraic equations that can be solved by standard linear-algebra techniques such as LU decomposition or iterative methods.

Despite their simplicity and transparency, FDMs suffer from the curse of dimensionality: in  $d$  dimensions the number of grid points grows exponentially with  $d$ . Consequently, their use is limited to small  $d$  or to cases where symmetry or decomposition can reduce the effective dimension.

## Monte Carlo Methods

Monte Carlo (MC) methods estimate prices by simulating many sample paths of the underlying assets under the risk-neutral measure  $\mathbb{Q}$  and averaging the discounted payoff [4]. With several risk factors this means generating correlated geometric Brownian motions. An example of an MC pricing algorithm is given below:

---

### Algorithm 1 MC pricing of a general payoff

---

- 1: **Input:** number of simulations  $N$ , horizon  $T$ , risk-free rate  $r$ , strike  $K$ , asset parameters  $(\mu_i, \sigma_i, \rho_{ij})$
- 2: **for**  $n = 1$  to  $N$  **do**
- 3:     Simulate one terminal price  $S_T^i$  for each asset using correlated Brownian increments
- 4:     Compute the payoff  $\text{Payoff}^{(n)}$
- 5: **end for**
- 6: Estimate the option value

$$V(0, \mathbf{S}_0) \approx e^{-rT} \frac{1}{N} \sum_{n=1}^N \text{Payoff}^{(n)}$$


---

MC methods are attractive in high dimensions because their convergence rate does not deteriorate with the number of state variables. They converge only at  $O(1/\sqrt{N})$ , however, so variance-reduction techniques (control variates, antithetic sampling, and so on) are usually needed for efficiency.

Another limitation is that plain MC simulation is ill-suited to early-exercise or strongly path-dependent derivatives, which require decisions at multiple dates or knowledge of the

full price path. Although extensions such as the Longstaff–Schwartz regression method [16] exist, they tend to be less accurate and less efficient than PDE-based approaches. In these situations, PINNs can offer a compelling alternative, as they tackle the pricing equation directly and naturally encode early-exercise or path-dependent features in the loss function.

### 3. PHYSICS-INFORMED MACHINE LEARNING

#### 3.1. Introduction to Physics-Informed Neural Networks (PINNs)

As noted in earlier sections, traditional numerical techniques for solving pricing PDEs often suffer from severe computational burdens that stem from complex payoff features or high dimensionality. Physics-Informed Neural Networks (PINNs), introduced by Raissi et al. [7], offer an alternative framework that embeds the governing PDE directly into the training process. Instead of relying solely on labelled data, PINNs enforce the physical laws and constraints intrinsic to the problem, thereby improving the accuracy, efficiency and robustness of the resulting approximation.

Consider a generic initial-boundary-value problem

$$\begin{aligned}\mathcal{N}_I[u(t, x)] &= 0, \quad x \in \Omega, \quad t \in [0, T], \\ \mathcal{N}_B[u(t, x)] &= 0, \quad x \in \partial\Omega, \quad t \in [0, T], \\ \mathcal{N}_0[u(t^*, x)] &= 0, \quad x \in \Omega, \quad t^* = 0,\end{aligned}\tag{3.1}$$

where  $\mathcal{N}_I$  is the interior operator on the spatial domain  $\Omega$ ,  $\mathcal{N}_B$  enforces the boundary conditions on  $\partial\Omega$ , and  $\mathcal{N}_0$  specifies the initial data.

A PINN approximates the solution  $u(t, x)$  by a neural network  $u_\theta(t, x)$  with parameters  $\theta$ . These parameters are determined by minimising the composite loss

$$\mathcal{L}(\theta) = \lambda_1 \mathcal{L}_{\text{PDE}}(\theta) + \lambda_2 \mathcal{L}_{\text{boundary}}(\theta) + \lambda_3 \mathcal{L}_{\text{initial}}(\theta),\tag{3.2}$$

where  $\lambda_i$  are predefined loss weights, and

$$\begin{aligned}\mathcal{L}_{\text{PDE}}(\theta) &= \int_0^T \int_{\Omega} |\mathcal{N}_I[u_\theta(t, x)]|^2 \, dx dt, \\ \mathcal{L}_{\text{boundary}}(\theta) &= \int_0^T \int_{\partial\Omega} |\mathcal{N}_B[u_\theta(t, x)]|^2 \, ds dt, \\ \mathcal{L}_{\text{initial}}(\theta) &= \int_{\Omega} |\mathcal{N}_0[u_\theta(0, x)]|^2 \, dx.\end{aligned}\tag{3.3}$$

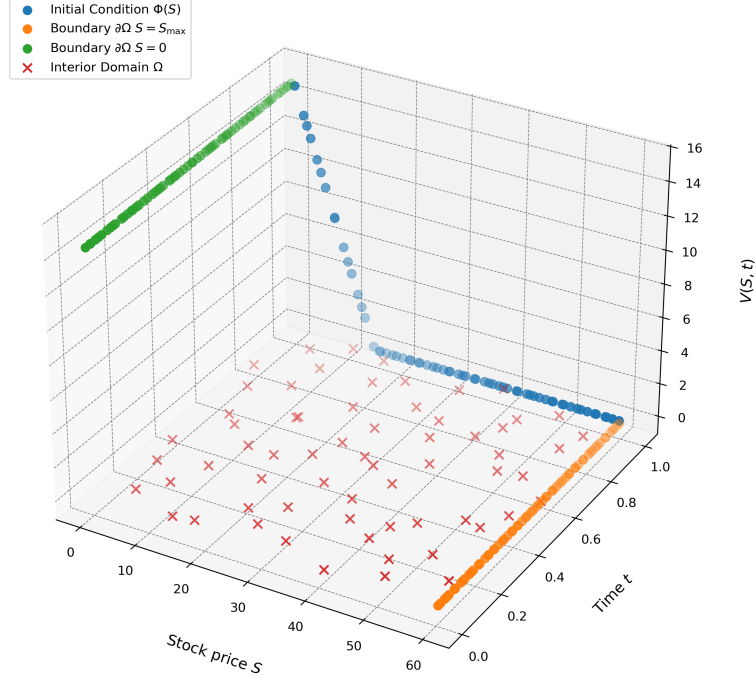
In practice these integrals are approximated via Monte Carlo sampling by evaluating the residuals at sets of collocation points drawn inside the corresponding domains.

#### 3.2. Training PINNs

Training PINNs entails minimising the total loss  $\mathcal{L}(\theta)$  with respect to the network parameters  $\theta$ . This is usually done with gradient-based optimisers such as stochastic gradient descent (SGD) and its variants, which iteratively update the parameters using the gradient

**Figure 3.1**

Collocation points for a put option. Points are sampled inside the domain  $\Omega$ , on the boundary  $\partial\Omega$ , and on the initial slice  $\Omega_0$ .



of the loss. An alternative is to employ quasi-Newton schemes—for example the L-BFGS algorithm—which approximate curvature through second-order information. These optimisers, however, are highly susceptible to ill-conditioning of the Hessian matrix, which can slow convergence or even cause divergence [17].

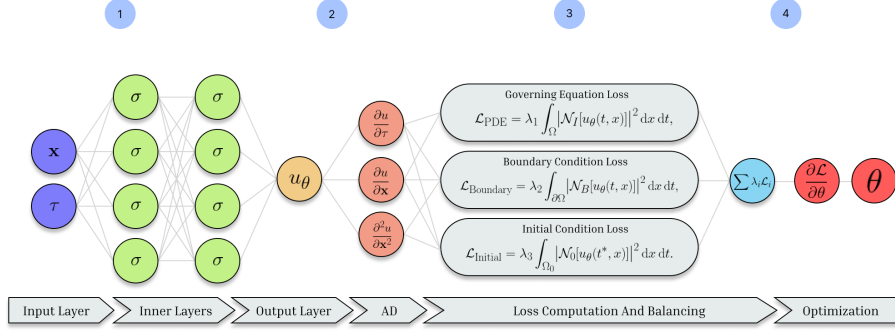
The required gradients are obtained by automatic differentiation, providing efficient and accurate sensitivities of the loss with respect to  $\theta$ . Iterations proceed until a stopping criterion is satisfied, such as a maximum number of steps or stabilisation of the loss value.

Because the exact solution is rarely available, training relies on synthetically generated collocation points sampled from the interior, boundary, and initial-condition domains. A common choice is uniform sampling over the relevant region.

Before optimisation, the parameters  $\theta$  are typically initialised randomly—often from a normal distribution with mean zero and small standard deviation—or taken from a suitable pre-trained model. Good initialisation is crucial for both convergence speed and final accuracy; the dimensionless reformulation of the PDEs introduced earlier helps by keeping input scales comparable [18].

**Figure 3.2**

Schematic of PINN training. (1) Collocation points are fed into the neural network. (2) Automatic differentiation yields spatial and temporal derivatives. (3) PDE residuals—and hence the loss terms—are evaluated at those points. (4) The resulting losses are combined to form  $\mathcal{L}(\theta)$ ; its gradient drives an optimisation step on  $\theta$ . The cycle repeats until convergence.




---

### Algorithm 2 Training procedure for a PINN

---

- 1: **Input:** network architecture; PDE, boundary, and initial operators.
  - 2: Initialise parameters  $\theta$ .
  - 3: Generate collocation points in  $\Omega$ ,  $\partial\Omega$ , and  $\Omega_0$ .
  - 4: **while** not converged **do**
  - 5:   (Optional) select a mini-batch of collocation points.
  - 6:   Evaluate the total loss  $\mathcal{L}(\theta)$  from (3.2).
  - 7:   Compute  $\nabla_\theta \mathcal{L}(\theta)$  via automatic differentiation.
  - 8:   Update  $\theta$  with the chosen optimiser.
  - 9: **end while**
- 

Fine-tuning any of these steps—sampling strategy, loss weights, optimiser choice, or learning-rate schedule—can materially improve performance. The next section outlines the configuration adopted in this thesis; implementation details follow in the subsequent chapter.

## 4. IMPLEMENTATION AND RESULTS

### 4.1. Implementation Details

Most of the results presented in this thesis use relatively small feedforward neural networks. These smaller architectures provided an optimal balance between computational efficiency and approximation accuracy. Regarding activation functions, we primarily employed the hyperbolic tangent ( $tanh$ ), given its smooth and differentiable nature. Although we also experimented with the Softplus activation—which closely resembles typical payoff functions—we observed only marginal improvements in convergence speed, insufficient to justify its use over  $tanh$ .

In terms of optimization methods, quasi-Newton algorithms, particularly the L-BFGS solver implemented in PyTorch, consistently delivered the best outcomes. Other solvers such as BFGS and SS-Broyden were also implemented and tested, and in some cases yielded better results. Gradient-based optimizers, notably Adam, were evaluated but generally failed to match the accuracy or convergence speed achieved by quasi-Newton approaches.

Sampling collocation points was predominantly carried out using a uniform distribution over the domain of interest to evaluate PDE residuals and boundary conditions. Alternative sampling strategies, including Sobol and Halton sequences, were tested but did not lead to significant improvements in accuracy or computational efficiency.

All models were implemented in Python using the PyTorch framework. The complete implementation is publicly available on GitHub [19]. Computations were performed on a personal computer equipped with an Intel i7-12700K CPU and an NVIDIA RTX 2070 GPU, facilitating efficient training of neural network models.

### 4.2. Call Option

As an initial test case for the methodology, we priced a standard European call option under the classical Black-Scholes model, whose PDE in Eq. (2.5) admits a closed-form solution that serves as a convenient benchmark. The numerical experiment used the parameters in Table 4.1.

Parameter	Value
Strike price, $K$	\$100
Maturity, $T$	1.0 year
Risk-free rate, $r$	0.05
Volatility, $\sigma$	0.20

**Table 4.1**  
*Call Option Parameters*

The physics-informed neural network (PINN) consisted of two hidden layers with 20 neurons each and was trained with the BFGS optimizer on 75000 collocation points distributed across the interior domain  $\Omega$ , the boundary  $\partial\Omega$ , and the initial hypersurface  $\Omega_0$ . Despite its simple architecture, the network reproduced the analytical solution accurately, achieving an  $L_2$  error of  $1.5054 \times 10^{-5}$ .

**Figure 4.1**  
*Call option price under the Black-Scholes PDE. The PINN solution closely matches the analytical benchmark.*

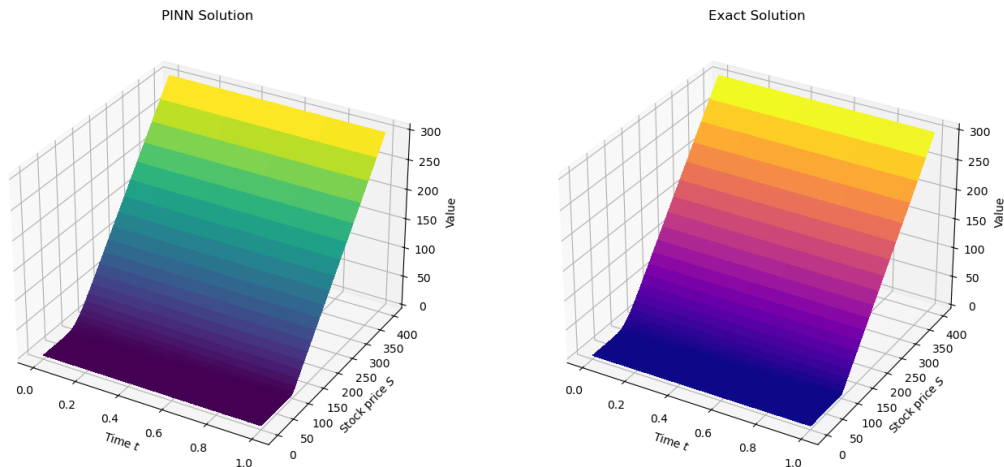
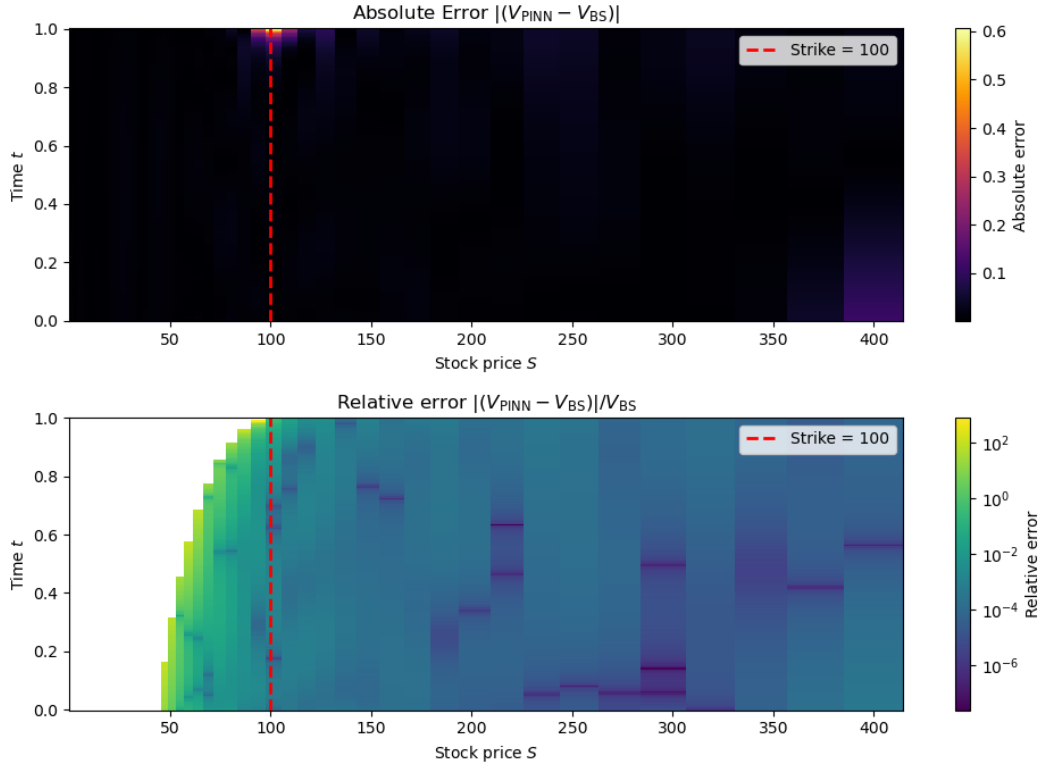


Figure 4.1 shows that the learned pricing surface is visually indistinguishable from the Black-Scholes benchmark, while Figure 4.2 depicts the absolute error, which is largest near maturity and the strike.

**Figure 4.2**

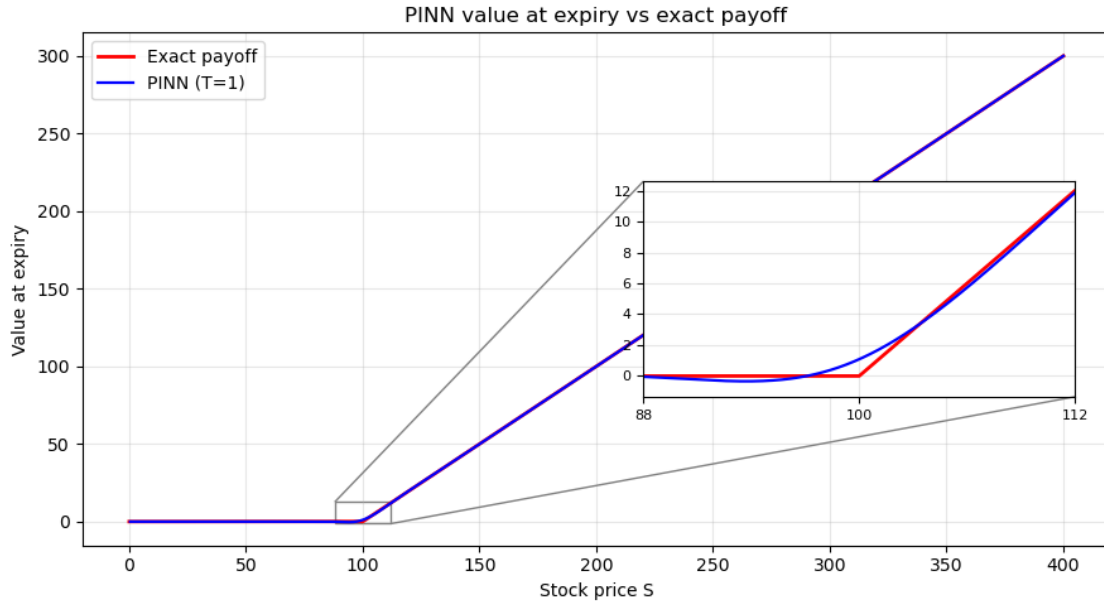
Absolute error of the PINN solution. Errors peak close to maturity and the strike price.



The pronounced spike in error around the strike at expiry originates from the kink in the payoff function. Approximating a function with a discontinuous first derivative by smooth basis functions (including neural networks) typically produces oscillatory overshoots near the non-smooth point; this behaviour is a manifestation of the *Gibbs phenomenon*.

**Figure 4.3**

*Solution at expiry. The PINN solution closely matches the analytical benchmark, except around the strike price where the absolute error peaks.*



The absolute error in Figure 4.4 highlights a limitation common to data-driven methods: reliability falls off when the model is evaluated outside the region covered by training points. Within the training domain, however, the accuracy is sufficient for professional use.

**Figure 4.4**

*Relative error of the PINN solution. The error is concentrated around the strike price and maturity.*



For this straightforward example, training required about two minutes, underscoring the computational burden that PINNs impose. Once trained, evaluation is fast—in our test, roughly 1.45× faster than the closed-form Black-Scholes formula—but the initial training cost remains a practical consideration.

### 4.2.1. Multi-Asset Option

To test the ability of PINNs to solve higher-dimensional problems, we extend the single-asset experiment to multiple underlying assets. A compact network with three hidden layers of ten neurons each is first trained on the dimensionless form of the multi-asset Black-Scholes PDE in Eq. (2.9).

Because training costs increase significantly with dimensionality—due both to the complexity of the boundary conditions and the exponential growth in the volume of the domain—we employ a deliberately small set of collocation points: 500 in the interior domain  $\Omega$ , 500 on the boundary  $\partial\Omega$ , and 500 on the initial hypersurface  $\Omega_0$ . It is important to note that the number of required points on the boundary increases linearly with the number of assets, which further contributes to the computational burden as dimensionality grows. The specific parameters used in this test case are summarized in Table 4.2.

Parameter	Value
Strike price, $K$	\$100
Maturity, $T$	1.0 year
Risk-free rate, $r$	0.05
Volatilities, $\sigma_i$	0.20
Correlation, $\rho_{ij}$	0.25

**Table 4.2**

*Multi-Asset Call Option Parameters*

The surfaces obtained from the trained PINN, shown in Figures 4.5 and 4.6, correspond to the first two asset dimensions in the dimensionless and original coordinate spaces, respectively.

As in the single-asset case, the solution displays the expected features: values near zero when asset prices are far below the strike, approximately linear growth as asset prices increase well above the strike, and a ridge or kink near the strike region. These qualitative features are preserved as dimensionality increases, but the quality of the approximation deteriorates. The surfaces reveal increased irregularity and loss of precision, particularly in regions near the domain boundaries.

**Figure 4.5**

Dimensionless multi-asset call option price (first two asset axes).

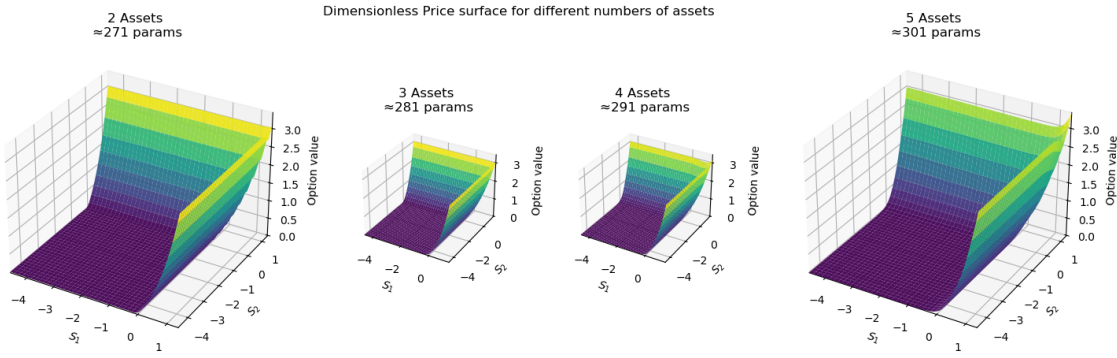
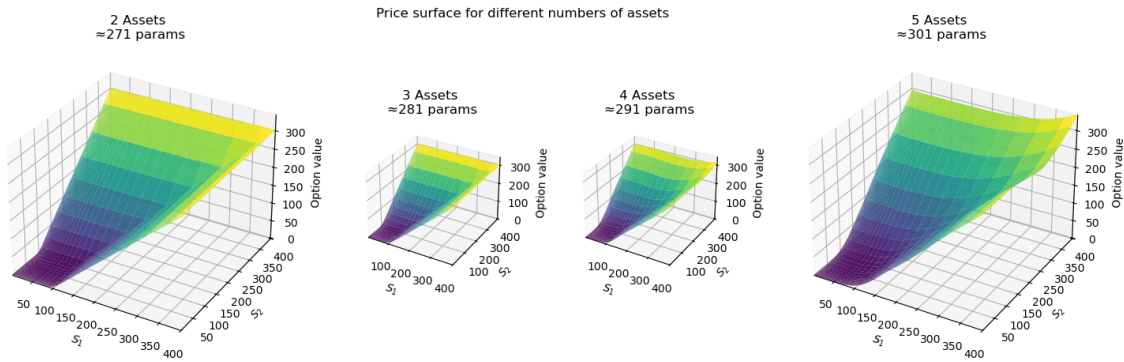


**Figure 4.6**

Multi-asset call option price in original coordinates (first two asset axes).

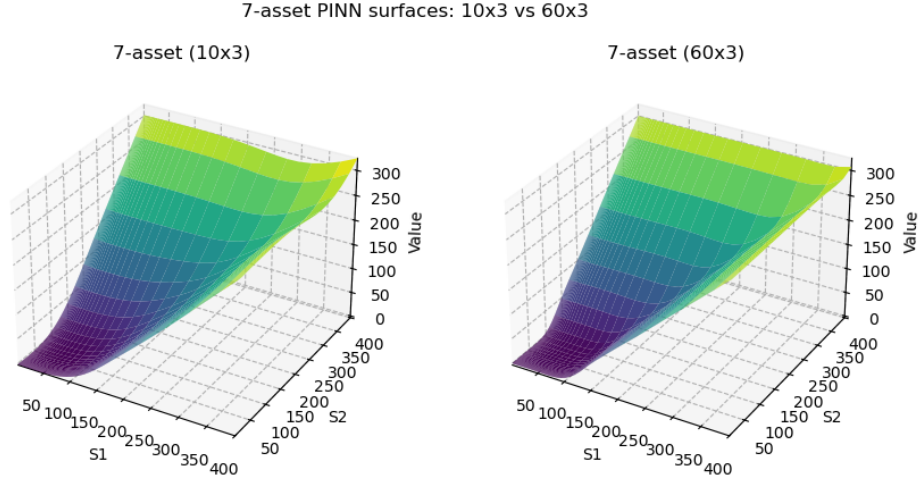


At the boundaries of the domain, especially in cases with more than three assets, the solution begins to exhibit an undesired curvature because the small network struggles to capture accurately the solution. In our experiments, increasing the number of boundary collocation points did not lead to significant improvements. Instead, better accuracy was achieved by increasing the expressiveness of the network.

By retaining the same number of layers but increasing the width to 60 neurons per layer, the network was able to represent the solution more faithfully, as demonstrated in Figure 4.7, which compares both architectures in a seven-asset configuration.

**Figure 4.7**

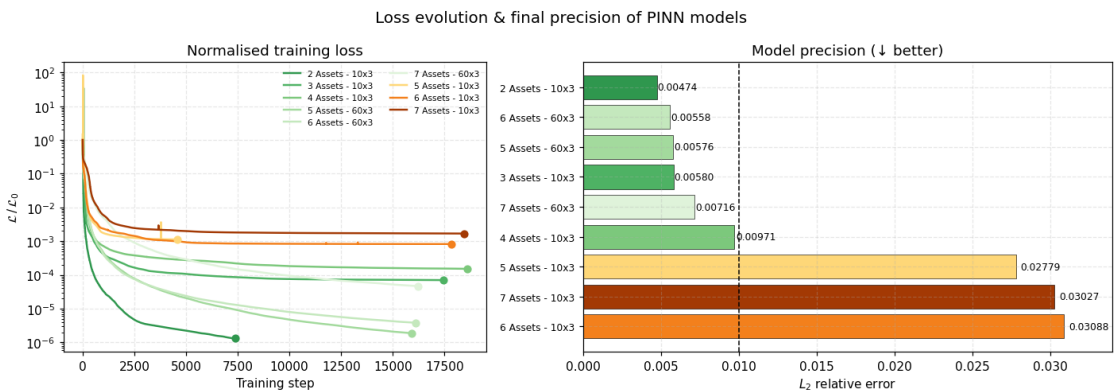
Seven-asset call option surfaces for two architectures. The network with 60 neurons per layer captures the solution more faithfully than the smaller 10-neuron model.



With the larger network and careful tuning of hyperparameters, it was possible to achieve a relative  $L_2$  error below  $10^{-3}$  (or better, depending on the case), which is generally considered acceptable for most practical applications. However, it is worth noting that such accuracy was not guaranteed across all dimensions and required repeated experimentation to achieve. Moreover, although the final error levels are satisfactory, there remains a lack of a comprehensive theoretical framework to rigorously bound the approximation error in higher dimensions. Figure 4.8 illustrates the convergence behaviour, where it is evident that larger networks converge more slowly but more reliably. In contrast, smaller networks occasionally terminate early due to reaching capacity limits, which may lead to misleadingly short training times but significantly worse solutions.

**Figure 4.8**

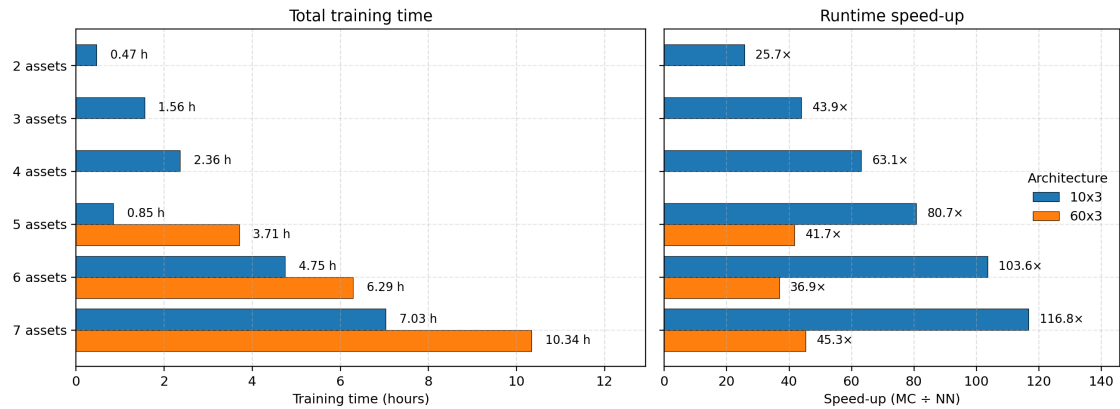
Training loss for multi-asset PINNs. Higher dimensions slow convergence and flatten the loss curve. The smaller network sometimes terminates early, yielding a shorter training time but a noticeably larger error.



Once trained, PINNs offer excellent performance in terms of computational speed. As shown in Figure 4.9, the inference time of a trained PINN is significantly faster than traditional Monte Carlo simulation methods, achieving substantial speedups even on a standard CPU. This computational advantage makes PINNs particularly attractive for real-time evaluations and repeated queries.

**Figure 4.9**

*CPU timing comparison between PINN inference and Monte Carlo simulation (50000 simulations).*



Despite the impressive inference speed, the long training times required for PINNs present a major limitation in professional financial settings. In practice, model parameters such as volatilities, correlations, and interest rates are frequently recalibrated to reflect changing market conditions.

Additionally, option-specific inputs such as strike prices and maturities may vary across instruments or need to be adjusted in scenario analyses. In such environments, it is common to perform rapid recalculations or sensitivity analyses, which demand flexible and responsive models. The requirement to retrain a PINN from scratch for each change in input parameters makes the method impractical for many real-time applications. To be viable in professional workflows, a PINN-based solution would either need to retrain extremely quickly, generalize across a wide range of parameter configurations, or be integrated selectively into systems that can tolerate delayed response times.

#### 4.2.2. Call Option with Stochastic Volatility and Interest Rates

We now extend our previous examples by introducing stochastic volatility and stochastic interest rates using the Heston-Hull-White model. This combined framework allows us to capture realistic market features, including volatility smiles and interest rate fluctuations. Figure 4.10 illustrates the price surfaces produced by the PINN under various volatility ( $\nu$ ) levels. The complete set of parameters used for this scenario is provided in Table 4.3.

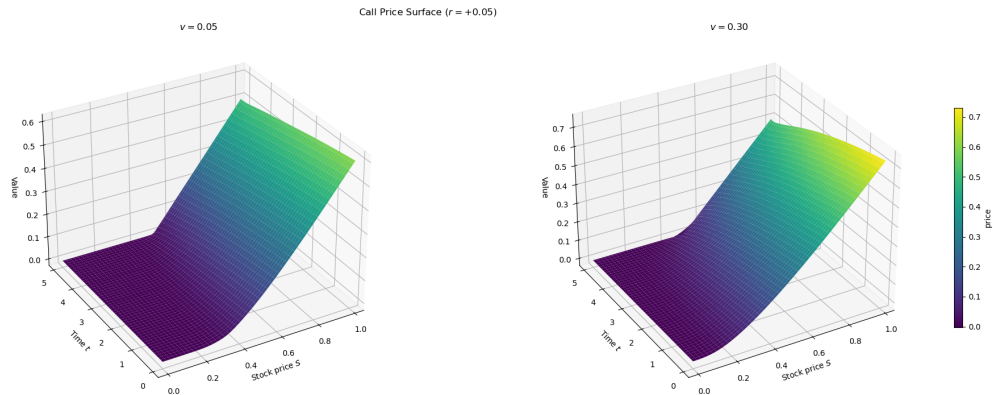
Parameter	Value
Strike price, $K$	\$0.5
Maturity, $T$	5.0 years
Initial risk-free short rate, $r_0$	0.05
Hull-White mean reversion speed, $a_r$	0.1
Hull-White mean reversion level, $\theta_r$	0.05
Hull-White interest rate volatility, $\sigma_r$	0.02
Heston initial volatility, $v_0$	0.04
Heston mean reversion speed, $\kappa_v$	1.5
Heston long-term volatility, $\theta_v$	0.04
Heston volatility of volatility, $\sigma_v$	0.2
Correlation between asset and volatility, $\rho_{Sv}$	-0.7
Correlation between asset and interest rate, $\rho_{Sr}$	0.0
Correlation between volatility and interest rate, $\rho_{vr}$	0.0

**Table 4.3**

Parameters for the Call Option under the Heston-Hull-White Model

**Figure 4.10**

Call option pricing surfaces using the Heston-Hull-White model for different volatility levels.

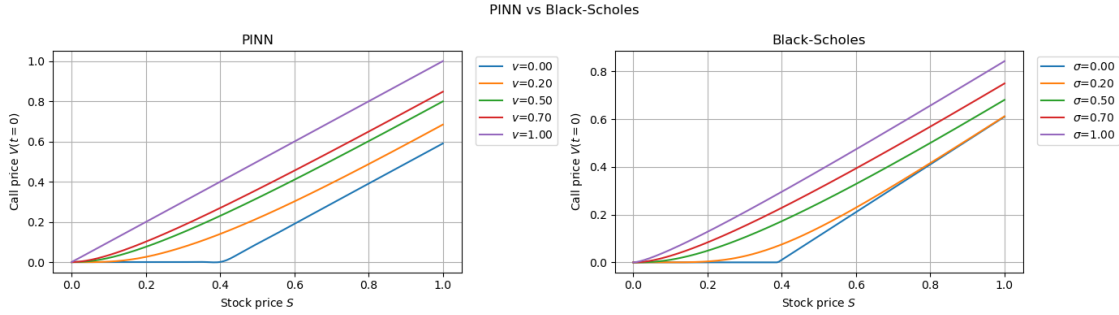


Using the experience from the case of Section 2.2.3, we used a neural network with three hidden layers, each containing 60 neurons, and trained it with the BFGS optimizer on 15000 collocation points distributed equitatively across the different domains.

Since no analytical solution exists for the combined Heston-Hull-White model, we qualitatively compare the PINN results to those obtained using the simpler Black-Scholes model (see Figure 4.11). It is possible to observe that for high underlying asset values, option prices behave nearly linearly with the underlying; at lower values, the price closely resembles the discounted payoff.

**Figure 4.11**

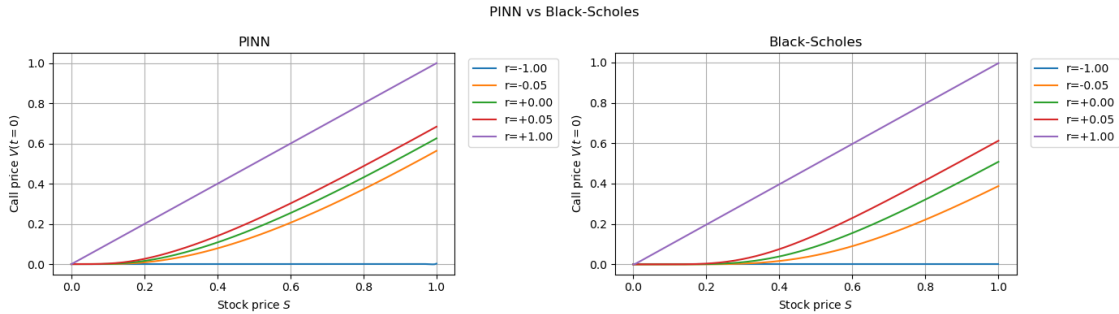
Price sensitivity to changes in volatility ( $v$ ). Higher values decrease curvature in the price surface.



The effect of interest-rate dynamics on option pricing is shown in Figure 4.12. As short-term interest rates increase, option prices generally rise, reflecting the increased cost associated with hedging positions and financing derivatives contracts over longer horizons. This aligns with standard market expectations.

**Figure 4.12**

Price sensitivity to short rates in the Heston-Hull-White model. Higher interest rates raise the option's hedging cost, increasing the option price.



As the model incorporates stochastic volatility and interest rates, the resulting price surfaces differ from the Black-Scholes solution, both because additional stochastic factors are present and because the combined model incorporates correlations between the underlying asset, volatility, and interest rates. This can be seen in Figure 4.13 and Figure 4.14, where the price surfaces are shown at  $t = 0$  for the stock and volatility dimensions, and the stock and interest rate dimensions, respectively.

**Figure 4.13**

Price surface at  $t = 0$  for the stock and volatility dimension.

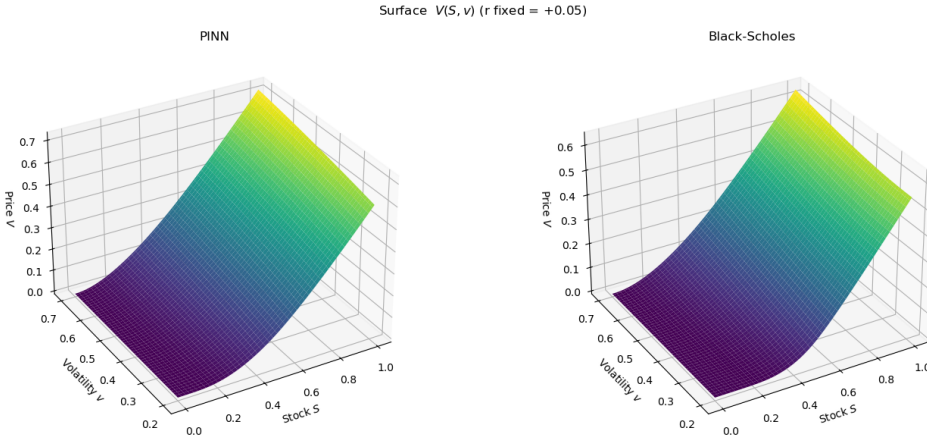
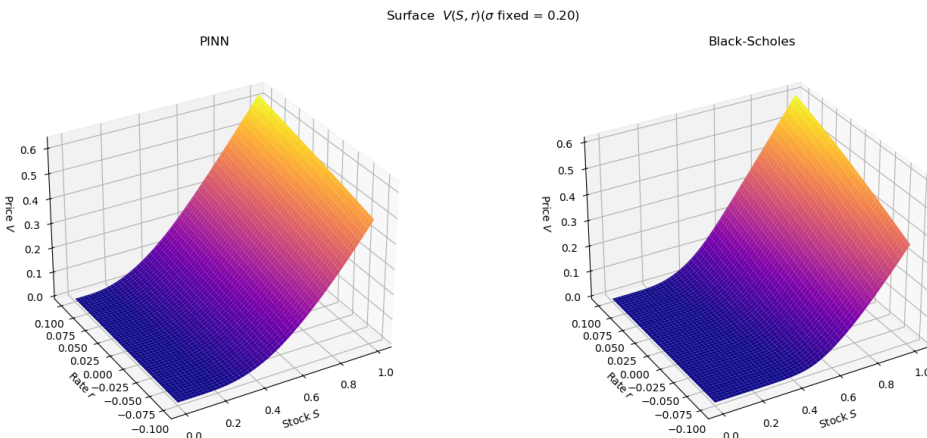


**Figure 4.14**

Price surface at  $t = 0$  for the stock and volatility dimension.



This experiment demonstrates that PINNs can accommodate richer dynamics than the Black-Scholes setting while retaining rapid inference once training is complete—a property valuable in latency-sensitive contexts such as high-frequency trading, where models must reconcile speed with the need to reflect joint dynamics.

### 4.3. Put Option Pricing

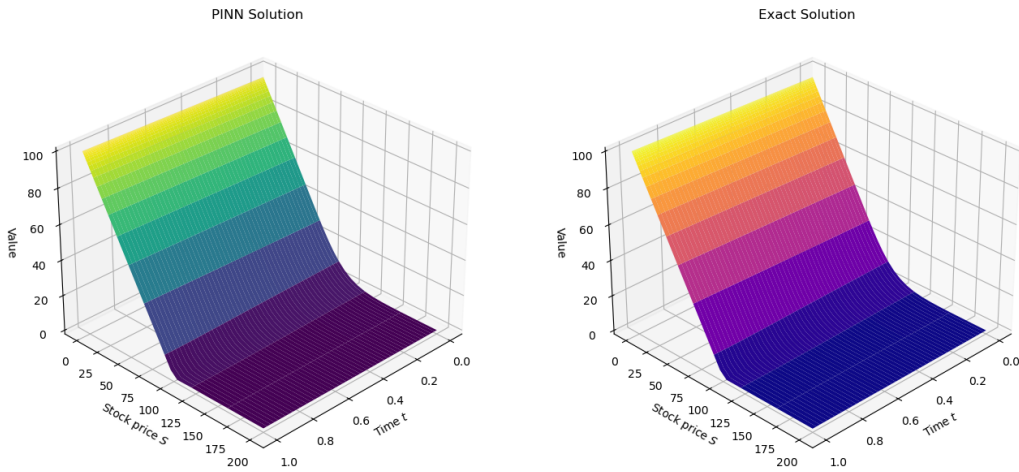
In this section, we aim to analyze early exercise features, where the most common example is the American put option, but we will also consider European put options for comparison. Puts are characterized by their distinct payoff function

$$\Phi(S) = \max(K - S, 0).$$

The pricing surface obtained from the PINN compared to the exact Black-Scholes analytical solution is displayed in Figure 4.15. Unlike call options, put option prices increase as the underlying asset value decreases, reflecting their payoff structure.

**Figure 4.15**

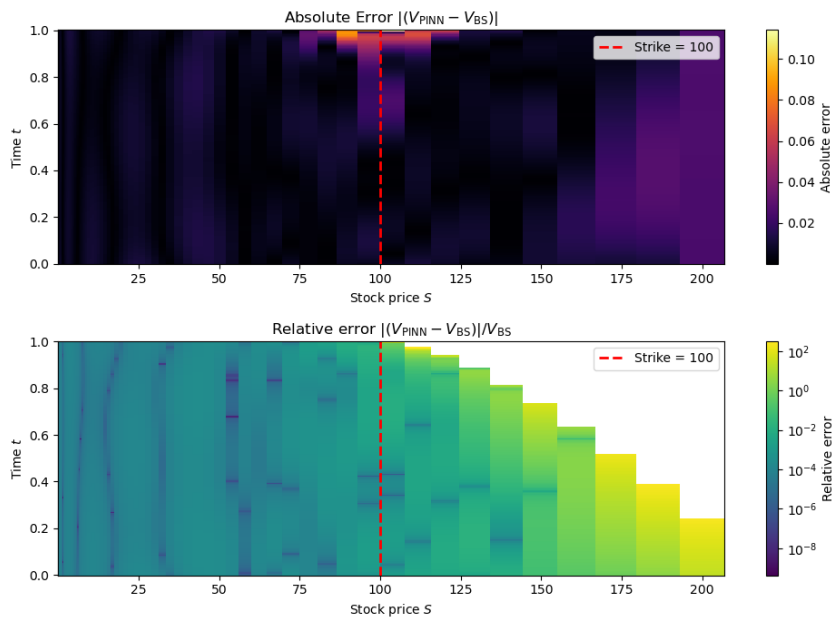
*European put option pricing: comparison between PINN (left) and analytical Black-Scholes solution (right).*



The absolute error in the put option pricing is shown in Figure 4.16, revealing error concentrations near maturity and around the strike price, consistent with the call option.

**Figure 4.16**

*Absolute error distribution for the European put option. Errors peak around maturity near the strike price.*



In this particular case, we limit our selves to state the  $L_2$  error obtained by the PINN,  $5.85 \times 10^{-5}$ , as the case is very similar to the call option.

### 4.3.1. American Put Option Pricing

An American put option introduces complexity due to its early-exercise feature, allowing the holder to exercise anytime before maturity. Consequently, pricing requires solving a free-boundary problem.

There are various ways to incorporate into the modeling framework free-boundary restrictions. In this experiment we achieve this by instead of directly minimizing the PDE interior residual ( $\mathcal{L}_{\text{PDE}}$ ), we minimize the following loss function:

$$\mathcal{L}_{\text{PDE}}(\theta) = \int_0^T \int_{\Omega} |\max\{\Phi(S) - u_{\theta}(t, x), N_I[u_{\theta}(t, x)]\}|^2 dx dt.$$

More on this can be found in [20], [21]. The resulting PINN solution, compared against a benchmark numerical solution (FDM), is shown in Figure 4.17.

**Figure 4.17**

American put option prices: PINN solution (left) compared to a numerical benchmark solution (right).

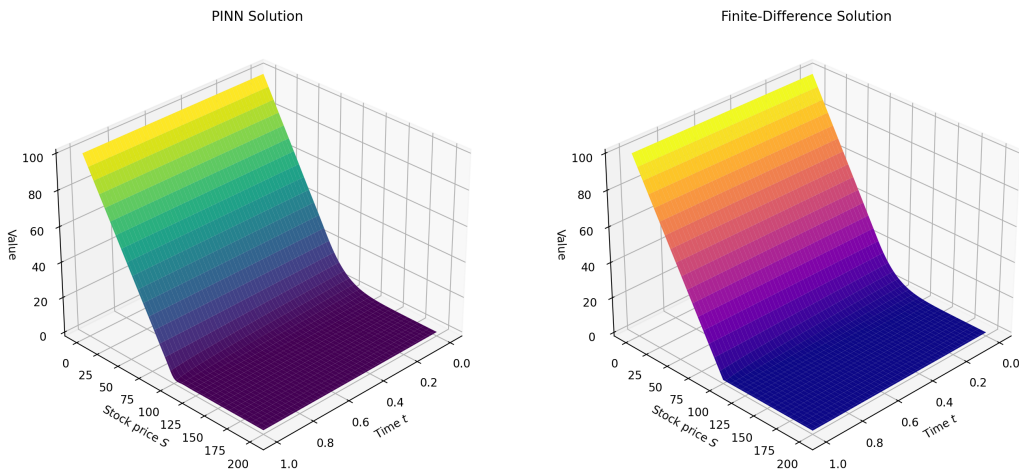
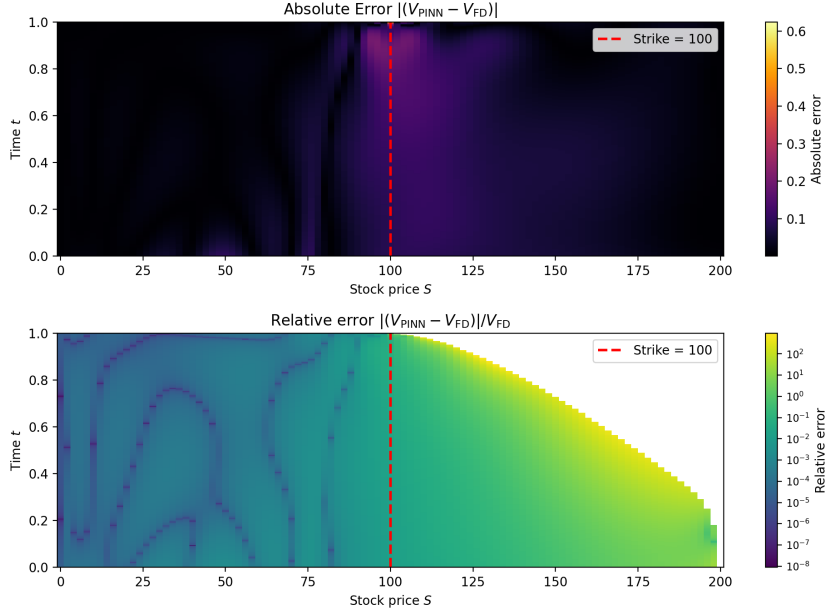


Figure 4.18 shows the absolute error in pricing the American put. The error is again concentrated around the strike price, though errors now extend across a wider region due to the early-exercise boundary's dynamic nature.

**Figure 4.18**

Absolute error for American put option pricing. Errors primarily arise around the dynamic early-exercise boundary.



In terms of the accuracy of the obtained solution, the PINN achieved an  $L_2$  error of  $1.30 \times 10^{-3}$ , which is acceptable for practical applications.

#### 4.4. Swaption Pricing

The final derivative instrument we evaluate is a European *payer swaption*, which gives the holder the right, but not the obligation, to enter into a fixed-for-floating interest rate swap at a specified future date. The underlying model used for pricing is the one-factor Hull-White model, as described in Section 2.2.5.

In this framework, the short rate  $r_t$  evolves according to the stochastic differential equation defined in 2.23. The swaption price depends on the future evolution of the short rate and on the value of the underlying swap, which itself is the present value of fixed versus floating rate payments over the swap's tenor.

**Figure 4.19**

European payer swaption pricing surface. Left: PINN solution. Right: reference solution computed with an analytic approximation or semi-analytical method.

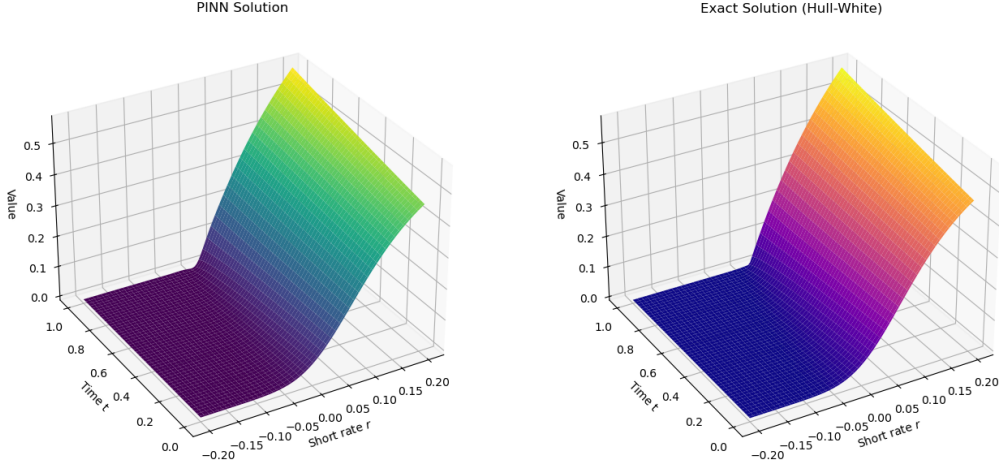
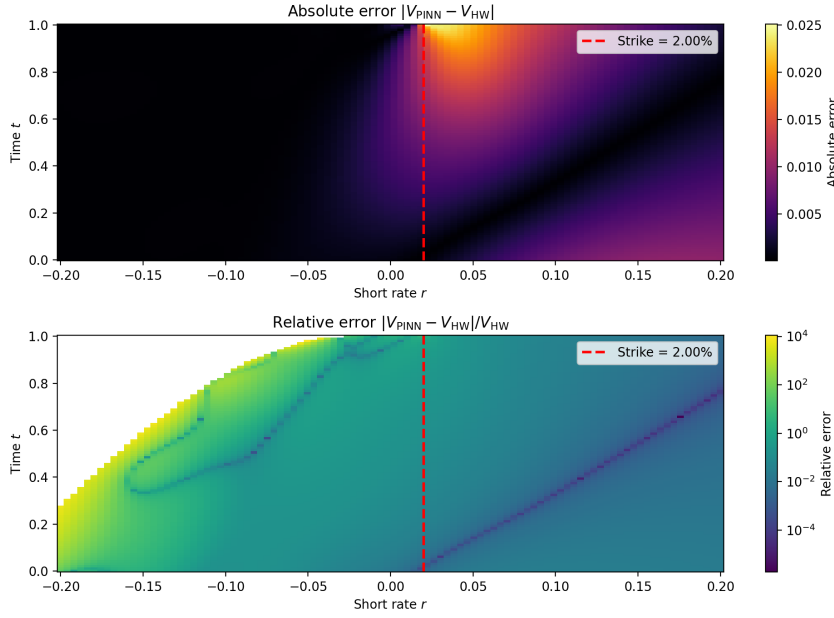


Figure 4.19 shows the pricing surface of a European swaption obtained using a PINN, compared against a benchmark solution from a conventional method. The neural network accurately captures the swaption price profile, particularly across key regions of the short-rate and strike axes. We deliberately choose a wide range for  $r$  to show the difference in the price surface, as it has non-linear features.

The absolute error of the PINN solution is shown in Figure 4.20. Most of the error is concentrated, again, near the strike region and close to expiry—areas where option payoffs exhibit low smoothness or where the valuation is highly sensitive to changes in rates.

**Figure 4.20**

Absolute error in pricing the European payer swaption. The error is primarily concentrated near expiry and around the strike.



For this particular case, the PINN achieved an  $L_2$  error of  $5.7 \times 10^{-3}$ . In general, the PINN demonstrates strong agreement with analytical benchmarks. This confirms its ability to handle the pricing of interest-rate derivatives with path-dependent structures and stochastic dynamics.

## **5. DISCUSSION, LIMITATIONS, AND OUTLOOK**

### **5.1. Discussion of the Main Findings**

## BIBLIOGRAPHY

- [1] Y. LeCun, Y. Bengio, and G. Hinton, “Deep learning,” *Nature*, vol. 521, pp. 436–44, May 2015. doi: [10.1038/nature14539](https://doi.org/10.1038/nature14539).
- [2] J. Hull, *Options, futures, and other derivatives*, eng, Ninth edition, Global edition. Boston: Pearson Education Limited, 2018 - 2018, ISBN: 1292212896.
- [3] P. Wilmott, “Paul wilmott on quantitative finance,” 2010. [Online]. Available: <https://api.semanticscholar.org/CorpusID:153668090>.
- [4] P. Glasserman, *Monte Carlo methods in financial engineering*. New York: Springer, 2004, ISBN: 0387004513 9780387004518 1441918221 9781441918222. [Online]. Available: [http://www.amazon.com/Financial-Engineering-Stochastic-Modelling-Probability/dp/0387004513/ref=pd\\_sim\\_b\\_68?ie=UTF8&refRID=1AN8JXSDGMEV2RPHFC2A](http://www.amazon.com/Financial-Engineering-Stochastic-Modelling-Probability/dp/0387004513/ref=pd_sim_b_68?ie=UTF8&refRID=1AN8JXSDGMEV2RPHFC2A).
- [5] F. Black and M. Scholes, “The pricing of options and corporate liabilities,” *Journal of Political Economy*, vol. 81, no. 3, pp. 637–654, 1973, ISSN: 00223808, 1537534X. [Online]. Available: <http://www.jstor.org/stable/1831029> (visited on 04/25/2025).
- [6] R. Bellman, “Dynamic programming,” *Science*, vol. 153, no. 3731, pp. 34–37, 1966.
- [7] M. Raissi, P. Perdikaris, and G. Karniadakis, “Physics-informed neural networks: A deep learning framework for solving forward and inverse problems involving non-linear partial differential equations,” *Journal of Computational Physics*, vol. 378, pp. 686–707, 2019, ISSN: 0021-9991. doi: <https://doi.org/10.1016/j.jcp.2018.10.045>. [Online]. Available: <https://www.sciencedirect.com/science/article/pii/S0021999118307125>.
- [8] S. L. Heston, “A closed-form solution for options with stochastic volatility with applications to bond and currency options,” *The Review of Financial Studies*, vol. 6, no. 2, pp. 327–343, 1993, ISSN: 08939454, 14657368. [Online]. Available: <http://www.jstor.org/stable/2962057> (visited on 07/06/2025).
- [9] B. Huge and A. Savine, *Differential machine learning*, 2020. arXiv: [2005.02347\[q-fin.CP\]](https://arxiv.org/abs/2005.02347). [Online]. Available: <https://arxiv.org/abs/2005.02347>.
- [10] J. B. Heaton, N. G. Polson, and J. H. Witte, *Deep learning in finance*, 2018. arXiv: [1602.06561 \[cs.LG\]](https://arxiv.org/abs/1602.06561). [Online]. Available: <https://arxiv.org/abs/1602.06561>.
- [11] F. Black and M. Scholes, “The pricing of options and corporate liabilities,” *Journal of Political Economy*, vol. 81, no. 3, pp. 637–654, 1973, ISSN: 00223808, 1537534X. [Online]. Available: <http://www.jstor.org/stable/1831029> (visited on 04/23/2025).

- [12] D. Duffy, *Numerical Methods in Computational Finance: A Partial Differential Equation (PDE/FDM) Approach* (Wiley Finance). Wiley, 2022, ISBN: 9781119719670. [Online]. Available: <https://books.google.es/books?id=6cZ6EAAQBAJ>.
- [13] D. Brigo and F. Mercurio, *Interest Rate Models Theory and Practice* (Springer Finance). Springer Berlin Heidelberg, 2013, ISBN: 9783662045534. [Online]. Available: <https://books.google.es/books?id=USvrCAAAQBAJ>.
- [14] O. Vasicek, “An equilibrium characterization of the term structure,” *Journal of Financial Economics*, vol. 5, no. 2, pp. 177–188, 1977, ISSN: 0304-405X. doi: [https://doi.org/10.1016/0304-405X\(77\)90016-2](https://doi.org/10.1016/0304-405X(77)90016-2). [Online]. Available: <https://www.sciencedirect.com/science/article/pii/0304405X77900162>.
- [15] J. Hull and A. White, “Pricing interest-rate-derivative securities,” *The Review of Financial Studies*, vol. 3, no. 4, pp. 573–592, Apr. 2015, ISSN: 0893-9454. doi: [10.1093/rfs/3.4.573](https://doi.org/10.1093/rfs/3.4.573). eprint: <https://academic.oup.com/rfs/article-pdf/3/4/573/24416170/030573.pdf>. [Online]. Available: <https://doi.org/10.1093/rfs/3.4.573>.
- [16] S. Longstaff, “Valuing american options by simulation: A simple least squares approach,” *Review of Finance Studies*, vol. 14, pp. 113–147, Jan. 2001.
- [17] J. F. Urbán, P. Stefanou, and J. A. Pons, “Unveiling the optimization process of physics informed neural networks: How accurate and competitive can pinns be?” *Journal of Computational Physics*, vol. 523, p. 113 656, Feb. 2025, ISSN: 0021-9991. doi: [10.1016/j.jcp.2024.113656](https://doi.org/10.1016/j.jcp.2024.113656). [Online]. Available: <http://dx.doi.org/10.1016/j.jcp.2024.113656>.
- [18] N. Malekjani, R. Kharaghani, and E. Tsotsas, “A comparative study of dimensional and non-dimensional inputs in physics-informed and data-driven neural networks for single-droplet evaporation,” *Chemical Engineering Science*, vol. 306, p. 121 214, Jan. 2025. doi: [10.1016/j.ces.2025.121214](https://doi.org/10.1016/j.ces.2025.121214).
- [19] J. Melo, *Leveraging physics-informed neural networks for option pricing problems*, [https://github.com/jmelo11/pricing\\_pinns](https://github.com/jmelo11/pricing_pinns), GitHub repository, accessed July 2025, 2025.
- [20] P. Wilmott, S. Howison, and J. Dewynne, *The Mathematics of Financial Derivatives: A Student Introduction* (The Mathematics of Financial Derivatives: A Student Introduction). Cambridge University Press, 1995, ISBN: 9780521497893. [Online]. Available: <https://books.google.es/books?id=VYVhnC3fIVEC>.
- [21] S. Ikonen and J. Toivanen, “Operator splitting methods for american option pricing,” *Applied Mathematics Letters*, vol. 17, no. 7, pp. 809–814, 2004, ISSN: 0893-9659. doi: <https://doi.org/10.1016/j.aml.2004.06.010>. [Online]. Available: <https://www.sciencedirect.com/science/article/pii/S0893965904804968>.